Spatial density oscillations in trapped dipolar condensates

H.-Y. Lu,[1] H. Lu,[2] J.-N. Zhang,[1] R.-Z. Qiu,[1] H. Pu,[2] and S. Yi[1]

[1]*Key Laboratory of Frontiers in Theoretical Physics, Institute of Theoretical Physics, Chinese Academy of Sciences, Beijing 100190, China*

[2]*Department of Physics and Astronomy, and Rice Quantum Institute, Rice University, Houston, Texas 77251, USA*

(Received 5 May 2010; published 30 August 2010)

We investigated the ground-state wave function and the free expansion of a trapped dipolar condensate. We find that dipolar interaction may induce both biconcave and dumbbell density profiles in the pancake- and cigar-shaped traps, respectively. In the parameter plane of the interaction strengths, the oscillating density profile in a harmonically trapped dipolar condensate occurs only when the interaction parameters fall into certain isolated areas. The relation between the positions of these areas and the trap geometry is explored. When a box potential is used to confine the condensate, spatial density oscillation becomes a generic feature. By studying the free expansion of the condensate with an oscillating density profile, we show that the spatial density oscillation is detectable from the time-of-flight image.

DOI: 10.1103/PhysRevA.82.023622 PACS number(s): 03.75.Hh, 03.75.Kk, 67.85.Jk

I. INTRODUCTION

Bose-Einstein condensates with dipole-dipole interaction have drawn significant interest over the past few years [1–3]. In particular, after the experimental observations of dipolar effects in Cr condensates [4] and in spin-1 Rb [5] condensates, the study of dipolar quantum gases is at the forefront of both theoretical and experimental research. Armed with the technique of Feshbach resonance, which tunes the short-range s-wave scattering length, experimentalists have investigated the stability and the anisotropic collapse of the Cr condensate [6,7]. In addition, dipolar effects have also been observed in condensates of K [8] and Li [9] atoms, which only possess small magnetic dipole moments. Because of the large electric dipole moment of the polar molecules, recent success in producing high phase-space-density gas of polar molecules [10,11] provides an even more promising platform for the study of the dipolar quantum many-body system.

The long-range and anisotropic characters of the dipolar interaction have a profound impact on the properties of quantum gases. For example, when loaded into an optical lattice, the long-range repulsive dipole-dipole interaction breaks the translational symmetry of the lattice such that the density wave phases can be formed [12,13]. In the presence of vortices [14] or a small perturbation in the trapping potential [15], the radial density profile of the condensate was found to develop oscillations. Of particular interest is that, even for a dipolar condensate confined in a single harmonic trap, a biconcave density profile can be found in a pancake-shaped trap [16,17]. In this case, the maximum density occurs at the periphery, instead of at the center, of the condensate, which resembles the shape of a red blood cell. Wilson *et al.* have proposed detection of the biconcave density profile by tuning the contact interaction to induce local collapse [18].

In the present paper, we systematically investigate the ground-state structure and the free expansion dynamics of a harmonically trapped dipolar condensate. For a given trap geometry, we map out the stability diagrams in the parameter plane of the interaction strengths. In addition to the biconcave condensates in oblate traps, a dipolar condensate may also have a dumbbell-shaped density profile in a prolate trapping potential. For simplicity, both biconcave and dumbbell density profiles are referred to as the spatial density oscillations (SDOs) in the condensates. In the stability diagram, SDO occurs only when the interaction strengths fall into certain isolated areas, which are called the density oscillation islands (DOIs). We also find the relation between the position of the DOIs and the trap geometry by fitting the numerical results. Finally, by studying the free expansion of the condensate with the oscillating density profile, we show that SDO can be detected in the time-of-flight image.

We will also consider a dipolar condensate trapped in box potentials. We show that the rigid walls of box potentials, in general, induce more pronounced SDO over a much larger region of the parameter space than harmonic potentials.

The remainder of this paper is organized as follows. In Sec. II, we briefly outline our model. In Sec. III, we introduce the numerical method used to compute the dipolar mean field. The numerical results on both the ground-state wave function of harmonically trapped dipolar condensates and the corresponding free expansion dynamics are presented in Sec. IV. In Sec. V, we discuss the enhanced SDO in a box potential. Finally, we conclude in Sec. VI.

II. FORMULATION

We consider a trapped condensate of N bosons with dipole moments $d\hat{z}$. Particles interact with each other via contact interaction V_0 and dipole-dipole interaction V_d. The total interaction potential takes the form

$$V(\mathbf{r}) = c_0\delta(\mathbf{r}) + fd^2\frac{1-3\cos^2\theta}{|\mathbf{r}|^3}, \tag{1}$$

where $c_0 = 4\pi\hbar^2 a_s/m$ with m as the mass of the particle and a_s as the s-wave scattering length tunable through Feshbach resonance, θ is the polar angle of $\mathbf{r}$, and $f \in [-\frac{1}{2},1]$ is a parameter continuously tunable via an orienting field, which rotates rapidly around the z axis [19]. The inclusion of the factor f makes the dipolar interaction between polarized dipoles tunable. For positive f, the dipolar force is repulsive (attractive) if two dipole moments are aligned side by side (head to tail). However, the opposite becomes true for negative f. Moreover, the trapping potential is assumed to be axially

symmetric,

$$U_{\rm ho}(\mathbf{r}) = \tfrac{1}{2}m\omega_\perp^2(x^2+y^2+\lambda^2 z^2),$$

where $\omega_\perp$ is the radial frequency and λ is the trap aspect ratio such that the axially frequency of the trap is $\omega_z = \lambda\omega_\perp$.

The condensate wave function satisfies the nonlocal Gross-Pitaevskii equation, which, in dimensionless form, becomes

$$i\frac{\partial\psi(\mathbf{r})}{\partial t} = \left[-\frac{1}{2}\nabla^2 + \frac{1}{2}(x^2+y^2+\lambda^2 z^2) + g|\psi(\mathbf{r})|^2 + D\int d\mathbf{r}'\frac{1-3\cos^2\theta}{|\mathbf{r}-\mathbf{r}'|^3}|\psi(\mathbf{r}')|^2\right]\psi(\mathbf{r}), \quad (2)$$

where $g = 4\pi Na/a_\perp$ and $D = Nfd^2/(\hbar\omega_\perp a_\perp^3)$ are the dimensionless parameters, which characterize the strengths of the contact and dipolar interactions, respectively. The dimensionless units adopted here are $a_\perp = \sqrt{\hbar/(m\omega_\perp)}$ for length, $\hbar\omega_\perp$ for energy, $\omega_\perp^{-1}$ for time, and $\sqrt{N/a_\perp^3}$ for wave function. In Eq. (2), the control parameters of the system are reduced to λ, g, and D. We will show how the condensate stability and the structure of the wave function depend on these parameters.

III. NUMERICAL METHOD

Following the standard procedure, the numerical solution of the ground-state wave function can be obtained by evolving Eq. (2) in imaginary time. Compared to the Gross-Pitaevskii equation with only the contact interaction, the difficulty of solving Eq. (2) lies at calculating the mean-field potential of the dipole-dipole interaction,

$$\Phi_d(\mathbf{r}) = \int d\mathbf{r}' V_d(\mathbf{r}-\mathbf{r}')n(\mathbf{r}') = \mathcal{F}^{-1}[\widetilde{V}_d(\mathbf{k})\tilde{n}(\mathbf{k})], \quad (3)$$

where $\mathcal{F}^{-1}$ denotes the inverse Fourier transform, $n(\mathbf{r}) = |\psi(\mathbf{r})|^2$ is the density of the condensate with $\tilde{n}(\mathbf{k})$ as its Fourier transform, and $\widetilde{V}_d(\mathbf{k}) = \frac{4\pi}{3}fd^2(3\cos^2\theta_k - 1)$ is the Fourier transform of the dipolar interaction potential with θ_k as the polar angle of $\mathbf{k}$. From the second line of Eq. (3), it becomes apparent that Φ_d can be efficiently calculated in momentum space by using fast Fourier transform (FFT) [2]. Moreover, by taking advantage of the cylindric symmetry of the system, Ronen *et al.* [20] further reduce the two-dimensional (2D) Fourier transform in the (x,y) plane into a one-dimensional Hankel transform of order 0 for the ground-state wave function by integrating over the azimuthal variable. This procedure greatly simplifies the three-dimensional (3D) calculation to a 2D one in the ρ-z plane.

The fact that FFT implicitly treats the system as a periodic one makes our system a 3D periodic lattice of condensates. Therefore, the dipolar interactions between the artificial periodic copies of condensates introduce error to the mean-field potential $\Phi_d(\mathbf{r})$. To solve this problem, Ronen *et al.* [16] suggest truncating the dipolar interaction such that V_d is nonzero only within a sphere of radius R, that is,

$$V_d^{(s)}(\mathbf{r}) = \begin{cases} fd^2(1-3\cos^2\theta)/r^3, & r < R, \\ 0, & \text{otherwise.} \end{cases} \quad (4)$$

This truncation of the dipolar interaction has no physical consequence as long as R is larger than the extent of the actual condensate, but it eliminates the interaction between artificial copies of condensates. This procedure works well in nearly spherical traps. However, for a cigar- or pancake-shaped trapping potential, one cannot find a sphere that only contains a single condensate. Here, a natural generalization is to introduce cylindrical truncation on the dipolar interaction potential:

$$V_d^{(c)}(\mathbf{r}) = \begin{cases} fd^2(1-3\cos^2\theta)/r^3, & |z| < Z \text{ and } \rho < R, \\ 0, & \text{otherwise.} \end{cases} \quad (5)$$

The Fourier transform of $V_d^{(c)}(\mathbf{r})$ takes the form

$$\frac{\widetilde{V}_d^{(c)}}{fd^2} = \frac{4\pi}{3}(3\cos^2\alpha - 1) + 4\pi e^{-Zk_\rho} \times [\sin^2\alpha\cos(Zk_z) - \sin\alpha\cos\alpha\sin(Zk_z)] - 4\pi\int_R^\infty \rho\, d\rho\int_0^Z dz\cos(k_z z)\frac{\rho^2-2z^2}{(\rho^2+z^2)^{5/2}}J_0(k_\rho\rho), \quad (6)$$

where $k_\rho = \sqrt{k_x^2+k_y^2}$, $\cos^2\alpha = k_z^2/(k_\rho^2+k_z^2)$, $J_0(\cdot)$ is the zeroth-order Bessel function. The first two lines on the right-hand side of Eq. (6) were previously obtained in Ref. [16], and the remaining integral term can easily be worked out by using numerical integration. With a Gaussian wave function, we have confirmed that the precision of the dipolar interaction energy is improved significantly by introducing cylindrical truncation on V_d.

Before we conclude this section, let us briefly summarize the numerical procedure employed to find the ground-state wave function of a dipolar condensate. For a given set of control parameters (λ, g, D), we first determine the proper values of R and Z. Then, by using Eq. (6), we numerically compute the Fourier transform of the modified dipolar interaction potential Eq. (6). Finally, by following the standard procedure for imaginary time evolution, we obtain the ground-state wave function.

IV. DIPOLAR CONDENSATES IN A HARMONIC TRAP

In this section, we will first map out the stability diagram of a trapped dipolar condensate in the parameter space (λ, g, D). The value of the trap aspect ratio λ ranges from 0.1 to 20, which covers both highly prolate and oblate trap geometries. For given parameters λ and D, to increase the repulsive contact interaction will stabilize the condensate; therefore, we manually set an upper limit on g such that $g \leqslant 600$. The lower limit of g, on the other hand, is introduced naturally as the system always becomes unstable by tuning the contact interaction to attractive with sufficiently large strength. Similarly, the lower and upper limits of the dipolar interaction strength are also determined by the stability of the condensate. In the second part of this section, we turn to study the free expansion dynamics of an initially trapped dipolar condensate, which aims at finding signatures of the SDO in time-of-flight images.

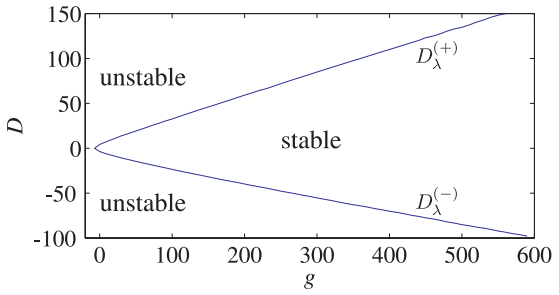

FIG. 1. (Color online) The stability diagram for $\lambda = 1$.

A. Stability diagram

In previous numerical studies [3,16,21], the stability diagram is plotted in a λ-D parameter plane for a given contact interaction strength g (which is usually taken to be zero). Here, for a fixed trap aspect ratio λ, we map out the stability diagram in a g-D parameter plane. As we will show later, this scheme makes it more convenient for us to understand the behavior of the SDO in a trapped dipolar condensate.

Figure 1 displays the stability diagram in a g-D parameter plane of a dipolar condensate in a spherical trap, which also represents the basic structure of the stability in other trap geometries. Since the dipolar force is partially attractive, a condensate always becomes unstable as the absolute value of D exceeds a certain threshold. In fact, for given g and λ, there exist two critical dipolar interaction strengths with opposite signs $D_\lambda^{(+)}(g) > 0$ and $D_\lambda^{(-)}(g) < 0$ such that the condensate is stable only if $D_\lambda^{(-)}(g) < D < D_\lambda^{(+)}(g)$. Alternatively, if D is fixed, the instability can also be induced by decreasing the scattering length (even to negative), similar to what has been done experimentally [7,22].

Moreover, when g (>0) is so large that the system falls into the Thomas-Fermi regime, the variational calculation shows that the stability boundary for given λ only depends on the ratio of D and g [21]. These properties are clearly reflected in Fig. 1, as for $g \gtrsim 100$, the critical D values linearly depend on g with slopes 0.255 and -0.151 for $D_\lambda^{(+)}$ and $D_\lambda^{(-)}$, respectively. The reason that the absolute value of $D_\lambda^{(+)}(g)$ is larger than $D_\lambda^{(-)}(g)$ is because, for spherical traps, the dipolar force with negative D is more attractive than that with positive D.

In general, the stability boundaries should depend on the trap aspect ratio λ. However, we find that, for positive (negative) D in a prolate (oblate) trap, the critical dipolar interaction strength is roughly independent of the trap geometry [i.e., $D_{\lambda>1}^{(-)}(g) \approx D_1^{(-)}(g)$ and $D_{\lambda<1}^{(+)}(g) \approx D_1^{(+)}(g)$]. In fact, under these conditions, the condensate shrinks as the dipolar interaction strength grows such that it only occupies a small spatial volume near the stability boundary. Therefore, the critical dipolar interaction strength becomes insensitive to λ. For this reason, we will focus on the upper stability boundary ($D_\lambda^{(+)}$) for oblate traps and the lower stability boundary ($D_\lambda^{(-)}$) for prolate traps.

In Fig. 2, we summarize the main results for the stability diagrams in oblate traps.When the interaction parameters fall into the shaded areas, a condensate possesses a biconcave density profile. The origin of the SDO can be intuitively understood as follows: the long-ranged dipolar interaction is repulsive in the xy plane; therefore, when the dipolar force exceeds a certain threshold value, the density at the center of the trap is depleted to lower the total energy. On the other hand, as one increases the dipolar interaction strength D, the attractive dipolar interaction along the z axis also becomes stronger, which destabilizes the system. In a slightly oblate trap, the system becomes unstable before such threshold dipolar force required from the SDO is reached. Therefore, for $\lambda \lesssim 3.2$, we do not find the biconcave density profile for g up to 600. To gain more insight into SDO, in Fig. 3(a), we plot the effective potential of the system:

$$U_{\rm eff}(\mathbf{r}) = U_{\rm ho}(\mathbf{r}) + g|\psi(\mathbf{r})|^2 + D\int d\mathbf{r}' V_d(\mathbf{r}-\mathbf{r}')|\psi(\mathbf{r}')|^2.$$

Apparently, when the density profile of the condensate becomes biconcave shaped in pancake-shaped traps, the effective potential takes the shape of a Mexican hat.

The first spatial density oscillations island (denoted as DOI-1) appears when $\lambda = 3.2$. Compared to the stability boundary, which corresponds to the normal density profile, it is clear that the critical dipolar interaction strength is slightly increased by forming a biconcave-shaped density profile in the condensate; and, away from the DOI, the $D_\lambda^{(+)}$ roughly linearly depends on g. As we increase λ, DOI-1 moves along the stability boundary to the negative direction of the g axis.

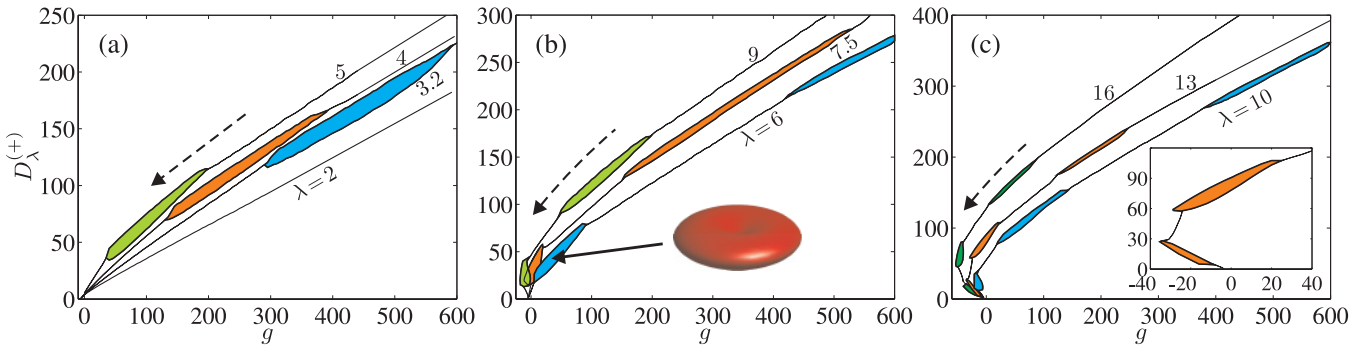

FIG. 2. (Color online) Contact interaction strength dependence of the upper critical dipolar interaction $D_\lambda^{(+)}$ for a condensate in pancake-shaped traps. The shaded areas mark the regions of parameter space where the biconcave condensates are found. The broken arrows denote the direction to which the DOIs move as λ is increased. The inset of (b) shows the typical isodensity surface of the condensate in the DOI. The inset of (c) reveals the detailed structure of the first two DOIs for $\lambda = 13$.

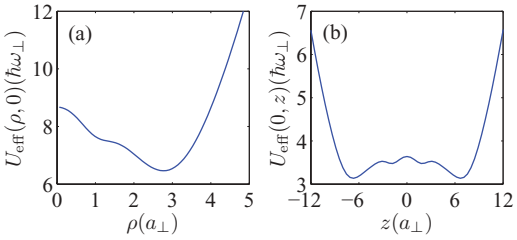

FIG. 3. (Color online) Effective potential $U_{\rm eff}(\rho,z)$ of the condensate in the presence of the SDO for (a) $(\lambda,g,D)=(8,-10,20)$ and (b) $(0.3,200,-49)$.

In addition, the area of DOI-1 shrinks. For even larger λ, the second (DOI-2) and the third (DOI-3) isolated parameter areas with SDO appear. They also move along the stability boundary by following the similar pattern as that of DOI-1 when the trap aspect ratio is increased.

A DOI can roughly be characterized by using the contact interaction strength: The range of g parameter covered by the DOI, where $\Delta g_{\rm DOI}$ represents its width; while the g value, at the center of this range $g_{\rm DOI}$, is the position of the DOI. Figure 4 shows the trap aspect ratio dependence of the positions of the three DOIs; the corresponding width is plotted as an error bar. One immediately notes that the λ dependence of $g_{\rm DOI}$ can be fitted by using the equation,

$$g_{\rm DOI}(\lambda)=\alpha e^{-\beta\lambda}-\gamma, \tag{7}$$

where the values of the fitting parameters α, β, and γ for different DOIs are listed in Table I. As shown in Fig. 4, the fitted curves agree very well with the numerical results for all DOIs. Moreover, the values of the fitting parameter γ also suggest that to increase λ will eventually push all three DOIs to the region with $g<0$. For large λ, all three DOIs are squeezed into a small region of g value, but they remain disconnected. We point out that, although Eq. (7) cannot explain why the DOIs appear under those contact interaction strengths, it can be used to predict the position of the DOIs.

As we will show in Sec. V, SDO can also be induced by the hard-wall boundary for a condensate trapped in a box potential, which can be explained as the manifestations of roton excitation [23,24]. In the harmonically trapped system, Ronen *et al.* [16] showed that the occurrence of the biconcave condensate coincides to the certain roton mode, which goes

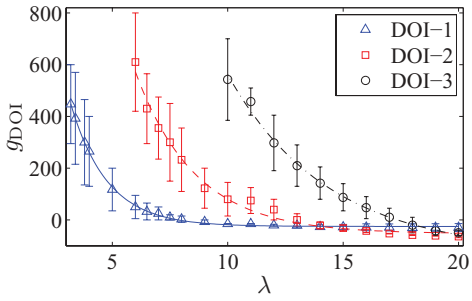

FIG. 4. (Color online) Trap aspect ratio dependence of the position and the width (represented by the length of the error bar) of the DOIs. The lines are plotted by using Eq. (7) with fitting parameters listed in Table I.

TABLE I. The values of fitting parameters for the positions of DOIs.

	α	β	γ
DOI-1	3559	0.6304	25.19
DOI-2	6328	0.3856	53.28
DOI-3	6933	0.2312	125.6

soft. Since the roton modes in the trapped system are discrete, SDOs can occur only when the parameters are such that they are resonant with the roton modes. For the given trap aspect ratio λ and the dipolar interaction strength D, the resonance condition can occur for certain values of the contact interaction strength g, which forms a discrete set of bands, which results in the DOIs observed in our numerical results. We note that a similar phenomenon occurs in the stability property of condensates with a multiply charged vortex [25]: Also, such a system only is stable in isolated regions along the g axis. For other values of the interaction strength g, the system becomes resonant with certain decay channels, which lead to instability islands. For the trapped dipolar system, when the trap aspect ratio λ is increased (i.e., when the trap becomes more oblate), the effective dipolar interaction becomes more repulsive. To soften the roton mode, the contact interaction strength has to be reduced. This explains why all the DOIs move to the negative direction along the g axis as λ is increased.

Once the position and width of a DOI are known, one may access the DOI by simply increasing the strength of the dipolar interaction strength to the value close to the critical value. In Fig. 5(a), we present the typical D dependences of the energies per particle.One immediately notices that the energies vary smoothly as the system enters the DOI, which indicates that condensates with and without SDO cannot be distinguished from each other by measuring the release energy. As shown in Fig. 5(b), for fixed D, one may also enter the DOI by lowering

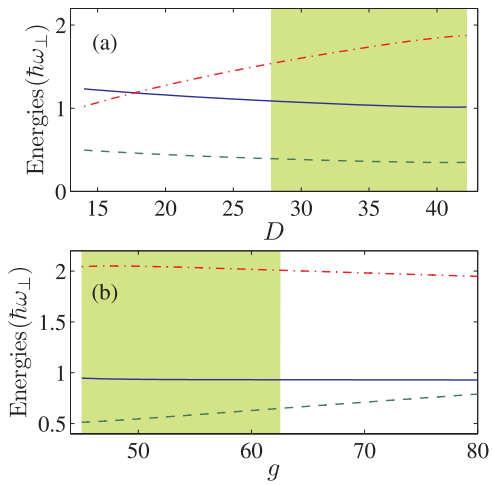

FIG. 5. (Color online) (a) Energies as functions of D for $\lambda=6$ and $g=25$. (b) Energies as functions of g for $\lambda=6$ and $D=55$. The solid, dashed, and dashed-dotted lines correspond to the kinetic, the contact interaction, and the dipolar interaction energies, respectively. The shaded area marks the range of the interaction parameters where the SDO appears.

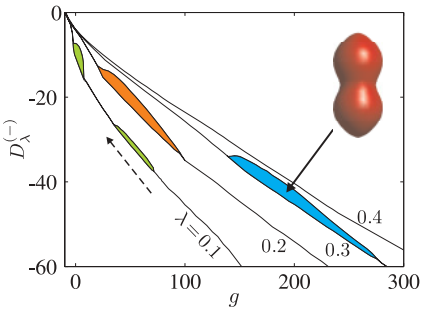

FIG. 6. (Color online) Contact interaction strength dependence of the upper critical dipolar interaction $D_\lambda^{(-)}$ for a condensate in cigar-shaped traps. The shaded areas mark the DOIs. The inset shows the typical result for the isodensity surface of the condensate. The broken arrows denote the direction to which the DOIs move as λ is decreased.

the contact interaction strength. Again, the energies are smooth functions of g across the boundary of a DOI.

The stability diagram of a dipolar condensate in cigar-shaped traps is presented in Fig. 6 where the DOIs appear when $\lambda \lesssim 0.3$.In contrast to the $D > 0$ case, the dipolar interaction becomes repulsive (attractive) along the axial (radial) direction for $D < 0$. Therefore, along the z direction, the repulsive dipolar force depletes the density at the center of the trap such that the isodensity surface of the condensate with SDO takes a dumbbell-shaped form. By corresponding to dumbbell structure, the effective potential [Fig. 3(b)] takes the form of a double-well potential. As the trapping potential becomes more pancake shaped, the DOIs move along the stability boundary to the negative direction of the g axis; in addition, the area of the DOI shrinks.

We remark that our results do not rule out the possibility that more DOIs might exist for larger g values, since our numerical calculations have only covered limited ranges of the parameters λ and g.

B. Free expansion

Now, we turn to study the expansion of initially trapped dipolar condensates. Compared to the contact interaction, the anisotropic nature of the dipolar interaction makes the expanded cloud behave quite differently [26–28]. Indeed, it has been used experimentally as a diagnostic tool for detection of the dipolar effects in Bose-Einstein condensates [4,8,9].

To study the free expansion dynamics, we consider an initially trapped condensate with control parameters (λ, g, D), which falls into a DOI. At time $t = 0$, we switch off the trapping potential; the expansion dynamics of the condensate is then described by Eq. (2) with $U_{\rm ho} = 0$. If the interactions are ignored completely during expansion, the condensate will expand ballistically such that the time-of-flight image represents the momentum distribution of the trapped condensate. From the Fourier transform of the initial wave function with SDO, one can easily deduce that two side peaks would appear in the time-of-flight image, which can be used as the signature of the oscillating density profile in the initial condensate.

To demonstrate this, we consider the expansion of an initially cigar-shaped condensate obtained by using the control parameter $(\lambda, g, D) = (0.2, 35, -18)$. Here, instead of tuning both g and D to zero, we only switch off the contact interaction for $t > 0$. Figure 7 shows the column densities of the expanded cloud, that is,

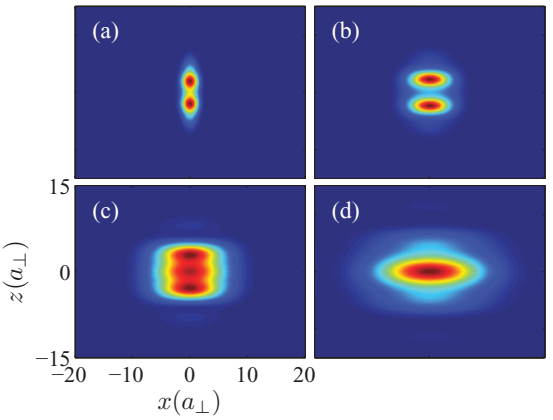

FIG. 7. (Color online) Column density of the expanded cloud for (a) $\omega_\perp t = 0$, (b) 3, (c) 5, and (d) 8. The initial states are obtained by using $(\lambda, g, D) = (0.2, 35, -18)$; during the expansion, g is tuned to zero.

$$\bar{n}(x,z,t) = \int dy\, n(x,y,z,t). \tag{8}$$

Due to the dumbbell-shaped density profile, the initial column density has two peaks analogous to that of the condensate trapped in a double-well potential. After the condensate expands such that these two peaks overlap, the third peak appears as a result of the interference. At time $\omega_\perp t = 5$, three peaks have roughly the same height. When the system evolves continuously, the heights of the two side peaks become lower and lower, but they are still visible at $\omega_\perp t = 8$. However, if the contact interaction remains unchanged during free expansion, the preceding scenario will be spoiled such that the side peaks will vanish very quickly for a cigar-shaped condensate.

Fortunately, for a pancake-shaped condensate, the side peaks of the column density remain visible for a long time if, initially, the dipolar interaction is very close to the stability boundary. In Fig. 8, we demonstrate the free expansion of a pancake-shaped condensate with an initial wave function obtained by using the control parameters $(\lambda, g, D) = (7, -5, 33)$. To make it easier to visualize the structure of the expanded cloud, we also plot the column density on the x axis. It can be seen that, even for $\omega_\perp t = 7$, the side peaks are still distinguishable from the column density, which indicates that the time-of-flight image may be used to detect the SDO in a dipolar condensate.

V. DIPOLAR CONDENSATE IN A BOX POTENTIAL

In this section, we briefly discuss the SDOs of a dipolar condensate trapped in a box potential. Specifically, we consider a potential that is harmonic along the z axis with frequency ω_z but is represented by infinite square wells with length L along the x and y axes. Such potential can be realized by using, for example, a tightly focused light sheet [29].

Figure 9 displays the stability diagram of such a system. As in the previous case, a critical dipolar interaction strength

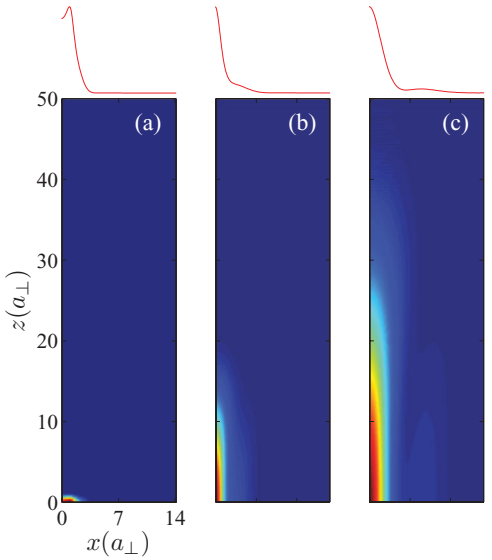

FIG. 8. (Color online) Column density of the expanded cloud for (a) $\omega_\perp t = 0$, (b) 3, and (c) 7. The curves at the upper row show the corresponding column density on the x axis [i.e., $\bar{n}(x,0)$]. The initial wave function is obtained by using the control parameters $(\lambda, g, D) = (7, -5, 33)$.

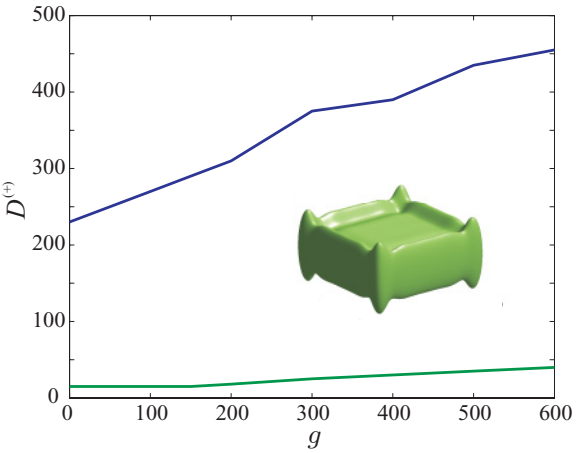

FIG. 9. (Color online) The upper solid line represents the upper critical dipolar interaction strength for a dipolar condensate confined in a box potential in the x-y plane and a harmonic potential in the z axis. The region between the lower and the upper solid lines represents regions where SDO will occur in the ground state. The inset shows an isodensity surface of a dipolar condensate with SDO. The length L along the x and y axes is taken to be $28a_z$, where $a_z = \sqrt{\hbar/(m\omega_z)}$. The dimensionless interaction strengths are defined as $g = 4\pi Na/a_z$ and $D = d^2/(\hbar\omega_z a_z^3)$.

exists beyond which the system will collapse. However, here, a rather significant difference is the much enlarged region of SDO. In fact, here, there are no disconnected DOIs, and SDO dominates a major portion of the parameter space. The inset of Fig. 9 exhibits a typical density plot of a condensate trapped in such a potential. One can easily see the pronounced oscillating density profiles near the walls.

That a hard wall induces SDOs in a dipolar condensate can be understood from the roton excitation of the system [15]. Here, the effect of the wall is not unlike a vortex line [14] or a localized repulsive potential [15]: They all represent localized perturbations that create a local superfluid density depression in the vicinity of which the roton mode becomes soft and manifests itself as SDOs [15]. The same physics also underlies the predicted density ripples in superfluid helium near a boundary [23] or a vortex line [24]. In the dipolar condensate, such perturbations are so strong that SDO occurs for any interaction strength g as long as the dipolar interaction strength is not too small.

From this study, one can conclude that SDOs in dipolar condensates can very easily be induced by a rigid wall. By contrast, in the case where the condensate is not confined in the x-y plane (which can be simulated by using the periodic boundary condition in the plane), we do not observe any SDOs—as dipolar interaction strength increases, the system remains uniform in the transverse plane until it collapses.

VI. CONCLUSION

To conclude, we have systematically investigated the SDOs in trapped dipolar condensates by mapping out the stability diagram of the system on a g-D parameter plane. In addition to the biconcave density profile in an oblate trap, the dipolar interaction can also generate dumbbell-shaped density profiles in prolate traps. On the stability diagram, the SDO occurred only when the interaction strengths fell into the DOIs. The relation between the positions of the DOIs and the trap geometry was explored by fitting the numerical results. We also studied the free expansion of the condensate with an oscillating density profile; it was shown that the SDO can be identified in the time-of-flight image. Finally, to improve the numerical precision for the calculation of dipolar interaction energy, we introduced the truncated dipolar interaction potential, which was nonzero only within a properly chosen cylinder.

ACKNOWLEDGMENTS

This work was supported by the NSFC through Grants No. 10974209 and No. 10935010 and by the National 973 program (Grant No. 2006CB921205). S.Y. acknowledges the support from the Bairen program of the Chinese Academy of Sciences. H.P. acknowledges the support from the NSF and the Welch Foundation (Grant No. C-1669).

[1] S. Yi and L. You, Phys. Rev. A **61**, 041604(R) (2000).
[2] K. Góral, K. Rzążewski, and T. Pfau, Phys. Rev. A **61**, 051601(R) (2000).
[3] L. Santos, G. V. Shlyapnikov, P. Zoller, and M. Lewenstein, Phys. Rev. Lett. **85**, 1791 (2000).
[4] J. Stuhler, A. Griesmaier, T. Koch, M. Fattori, T. Pfau, S. Giovanazzi, P. Pedri, and L. Santos, Phys. Rev. Lett. **95**, 150406 (2005).
[5] M. Vengalattore, S. R. Leslie, J. Guzman, and D. M. Stamper-Kurn, Phys. Rev. Lett. **100**, 170403 (2008).

[6] T. Koch, T. Lahaye, J. Metz, B. Frohlich, A. Griesmaier, and T. Pfau, Nat. Phys. **4**, 218 (2008).
[7] T. Lahaye, J. Metz, B. Frohlich, T. Koch, M. Meister, A. Griesmaier, T. Pfau, H. Saito, Y. Kawaguchi, and M. Ueda, Phys. Rev. Lett. **101**, 080401 (2008).
[8] M. Fattori, G. Roati, B. Deissler, C. D'Errico, M. Zaccanti, M. Jona-Lasinio, L. Santos, M. Inguscio, and G. Modugno, Phys. Rev. Lett. **101**, 190405 (2008).
[9] S. E. Pollack, D. Dries, M. Junker, Y. P. Chen, T. A. Corcovilos, R. G. Hulet, Phys. Rev. Lett. **102**, 090402 (2009).
[10] S. Ospelkaus, A. Pe'er, K.-K. Ni, J. J. Zirbel, B. Neyenhuis, S. Kotochigova, P. S. Julienne, J. Ye, and D. S. Jin, Nat. Phys. **4**, 622 (2008).
[11] K.-K. Ni, S. Ospelkaus, M. H. G. de Miranda, A. Pe'er, B. Neyenhuis, J. J. Zirbel, S. Kotochigova, P. S. Julienne, D. S. Jin, and J. Ye, Science **322**, 231 (2008).
[12] K. Góral, L. Santos, and M. Lewenstein, Phys. Rev. Lett. **88**, 170406 (2002).
[13] S. Yi, T. Li, and C. P. Sun, Phys. Rev. Lett. **98**, 260405 (2007).
[14] S. Yi and H. Pu, Phys. Rev. A **73**, 061602(R) (2006).
[15] R. M. Wilson, S. Ronen, J. L. Bohn, and H. Pu, Phys. Rev. Lett. **100**, 245302 (2008).
[16] S. Ronen, D. C. E. Bortolotti, and J. L. Bohn, Phys. Rev. Lett. **98**, 030406 (2007).
[17] O. Dutta and P. Meystre, Phys. Rev. A **75**, 053604 (2007).
[18] R. M. Wilson, S. Ronen, and J. L. Bohn, Phys. Rev. A **80**, 023614 (2009).
[19] S. Giovanazzi, A. Görlitz, and T. Pfau, Phys. Rev. Lett. **89**, 130401 (2002).
[20] S. Ronen, D. C. E. Bortolotti, and J. L. Bohn, Phys. Rev. A **74**, 013623 (2006).
[21] S. Yi and L. You, Phys. Rev. A **63**, 053607 (2001).
[22] T. Lahaye, T. Koch, B. Fröhlich, M. Fattori, J. Metz, A. Griesmaier, S. Giovanazzi, and T. Pfau, Nature (London) **448**, 672 (2007).
[23] T. Regge, J. Low Temp. Phys. **9**, 123 (1972).
[24] F. Dalfovo, Phys. Rev. B **46**, 5482 (1992).
[25] H. Pu, C. K. Law, J. H. Eberly, and N. P. Bigelow, Phys. Rev. A **59**, 1533 (1999).
[26] S. Yi and L. You, Phys. Rev. A **67**, 045601 (2003).
[27] S. Giovanazzi, A. Gorlitz, and T. Pfau, J. Opt. B: Quantum Semiclassical Opt. **5**, S208 (2003).
[28] S. Giovanazzi, P. Pedri, L. Santos, A. Griesmaier, M. Fattori, T. Koch, J. Stuhler, and T. Pfau, Phys. Rev. A **74**, 013621 (2006).
[29] T. P. Meyrath, F. Schreck, J. L. Hanssen, C.-S. Chuu, and M. G. Raizen, Phys. Rev. A **71**, 041604(R) (2005).